The Excited State Potential Energy Surface for the Photoisomerization of Tetraphenylethylene: A Fluorescence and Picosecond Optical Calorimetry Investigation

Jangseok Ma,[†] G. Bhaskar Dutt,[‡] David H. Waldeck,*[,‡] and Matthew B. Zimmt*[,†]

Contribution from the Departments of Chemistry, Brown University, Providence, Rhode Island 02912, and University of Pittsburgh, Pittsburgh, Pennsylvania 15260

Received May 23, 1994[⊗]

Abstract: A rudimentary map of the photoisomerization potential energy surface for tetraphenylethylene in alkane solvents is experimentally determined. The line shapes of the vertical and relaxed excited states emissions at 294 K in methylcyclohexane are obtained from the steady state emission spectrum and the wavelength dependence of the time resolved fluorescence decays. Subsequently, the temperature dependences of the vertical and relaxed states emission quantum yields and of the time resolved fluorescence decays are determined. Analysis of these data in conjunction with the twisted excited state energy, determined using picosecond optical calorimetry, provides values for the energies of the vertical, conformationally relaxed, and twisted excited states on the photoisomerization surface, as well as the barriers to their interconversion. The energy difference between the latter two states is found to be 1.76 ± 0.15 kcal/mol in methylcyclohexane. The information from this and prior investigations is discussed with the aim of constructing structure–energy and structure–kinetic correlations for the twisted excited states of tetraphenylethylenes and structurally related alkenes.

I. Introduction

Olefin photoisomerization reactions play important roles in organic photochemistry[1] and chemical physics.[2] The archetypal examples of such reactions are the photoisomerization of *cis*- and *trans*-stilbene and their analogs.[1,2] An enormous variety and number of experimental techniques have been used in the effort to understand the excited state dynamics in these systems. Much of this work has been reviewed recently.[2] A major need remaining for these studies is a more detailed and accurate understanding of the excited state potential energy surface(s) in the reaction. A primary limitation is the small amount of information available concerning the twisted excited singlet state, also called the phantom state, ^{1}p*. Little is known about this state in stilbene because of its very short lifetime, ca. 200 fs or shorter.[3] By contrast, the twisted excited singlet state of the stilbene analog, tetraphenylethylene (**1**), is quite long lived, thus making it possible to characterize the potential energy surface in the vicinity of the twisted excited state. It is this molecule and its alkyl-substituted analogs that are the subjects of this study.

In 1981, Barbara, Rand, and Renzepis[4] reported picosecond time resolved fluorescence studies of the dynamics of tetraphenylethylene (**1**) under a variety of conditions. Their work demonstrated the formation of at least two distinct emissive species *prior* to the formation of the twisted excited singlet state. These two species were identified as the nascent conformation, generated by vertical excitation of the ground state, ^{1}V, and a conformationally relaxed structure, ^{1}R. The involvement of two emissive conformations provided additional insight into the dependence of the fluorescence quantum yield on viscosity and temperature.[5] Also in 1981, Greene[6] reported the picosecond formation and nanosecond decay of a transient absorption produced by irradiation of **1** in hexane. This transient was assigned as the ^{1}p* state of **1**.

In 1988, Schilling and Hilinski[7] reported that the ^{1}p* state lifetime of **1** decreases rapidly in solvents of increasing solvent polarity. They explained this solvent dependence by postulating substantial zwitterionic character in the ^{1}p* state; i.e., this electronic state has a large contribution from a configuration described as a diphenylmethyl anion and a diphenylmethyl cation. Additional support for the zwitterionic nature of the twisted excited state was obtained by comparing the observed transient absorption spectrum to the spectrum of a mixture of the diphenylmethyl anion and cation. A second piece of evidence supporting zwitterionic character in the ^{1}p* state of **1** was provided by picosecond optical calorimetry studies.[8] The energy of the ^{1}p* state was determined to be 67 kcal/mol in alkane solvents and 65 kcal/mol in tetrahydrofuran. An analysis of this solvent dependent ^{1}p* state energy indicated the presence of a 6 D dipole moment. A picosecond transient absorption study of **1** in supercritical fluids provided additional evidence for charge separation in the ^{1}p* state.[9] Definitive evidence of zwitterionic character in the ^{1}p* state of **1** was provided by a time resolved microwave conductivity study,[10] in which a minimum value of 7.5 D for the dipole moment was reported. This collective evidence strongly supports the presence of charge separation in the twisted excited singlet state of **1**.

Analysis of the nanosecond time resolved fluorescence decays observed in two investigations[10,11] has demonstrated that the ^{1}p* state is not formed irreversibly from the fluorescent states studied by Barbara et al.[4] Rather, equilibration between the

[†] Brown University.
[‡] University of Pittsburgh.
[⊗] Abstract published in *Advance ACS Abstracts*, October 1, 1994.

(1) (a) Saltiel, J.; D'Agostino, J.; Megarity, E. D.; Metts, L.; Neuberger, K. R.; Wrighton, M.; Zafiriou, O. C. *Organic Photochemistry*; Chapman, O. L., Ed.; Marcel Dekker: New York, 1973; Vol. 3. (b) Saltiel, J.; Sun, Y. P. *Photochromism—Molecules and Systems*; Durr, H., Bouas-Laurent, H., Eds.; Elsevier: Amsterdam, 1990; p 64.
(2) Waldeck, D. H. *Chem. Rev.* **1991**, *91*, 415.
(3) Sension, R. J.; Repinec, S. T.; Szarka, A. Z.; Hochstrasser, R. M. *J. Chem. Phys.* **1993**, *98*, 6291.
(4) Barbara, P. F.; Rand, S. D.; Rentzepis, P. M. *J. Am. Chem. Soc.* **1981**, *103*, 2156.
(5) Sharafy, S.; Muszkat, K. A. *J. Am. Chem. Soc.* **1971**, *93*, 4119.
(6) Greene, B. I. *Chem. Phys. Lett.* **1981**, *79*, 51.
(7) Schilling, C. L.; Hilinski, E. F. *J. Am. Chem. Soc.* **1988**, *110*, 2296.
(8) Morais, J.; Ma, J.; Zimmt, M. B. *J. Phys. Chem.* **1991**, *95*, 3885.
(9) Sun, Y.-P.; Fox, M. A. *J. Am. Chem. Soc.* **1993**, *115*, 747.

0002-7863/94/1516-10619$04.50/0

Scheme 1

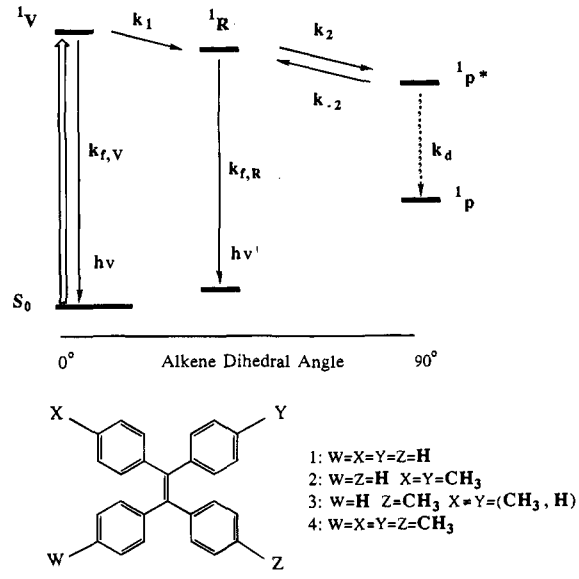

conformationally relaxed emissive state, ^1R, and the $^1p^*$ state was achieved in hydrocarbon solvents. The existence of this equilibrium, in conjunction with previous studies, provides a means to determine the energies of all three excited state species, ^1V, ^1R, and $^1p^*$, as well as the barriers impeding their interconversions. This paper reports the results of studies that aim to experimentally map the excited state potential energy surface of **1** in alkane solvents. In addition, calorimetric characterization of the $^1p^*$ state energies in alkyl-substituted derivatives of **1** are described and are used to generate structure–energy correlations for twisted excited singlet states of these and other alkenes. Very recently time resolved Raman[12] studies of **1** and fluorescence studies in supercritical media[13] have appeared. The latter study reports the line shapes of both the ^1V and ^1R emissions from **1**, which were obtained using different supercritical media. The disection of experimental fluorescence spectra into contributions from the ^1V and ^1R species plays a central role in this study, although a different approach is used to effect the separation.

The kinetic model used to analyze the fluorescence spectra and dynamics from **1** is shown in Scheme 1. Photon absorption generates the vertical excited state, which decays by two pathways: fluorescence, which proceeds with the rate constant $k_{f,V}$, and a conformational relaxation, which produces the ^1R state with a rate constant k_1. The relaxed state decays by fluorescence, with rate constant $k_{f,R}$, and by a second structural relaxation that produces the twisted excited state with a rate constant k_2. In the $^1p^*$ state, the dihedral angle between the two planes defined by the ethylenic carbons and the carbons of the aryl groups to which each is bonded is taken to be 90°. Two decay channels are available to the $^1p^*$ state: (i) radiationless decay to the ground state surface, characterized by the decay rate constant k_d, and (ii) thermal repopulation of the ^1R state, which occurs with the rate constant k_{-2}. The ^1R state lies higher in energy than the $^1p^*$ state by the amount ΔE. With the exception of the radiative processes, the temperature dependence of each rate constant within Scheme 1 is assumed to obey the Arrhenius equation. It should be noted that the description of the three excited species as "states" is not intended to indicate non-adiabaticity in their interconversions.

Using this model, the steady state emission spectrum and the wavelength dependence of the time resolved fluorescence will be used to determine the shapes and quantum yields of the ^1R and ^1V emissions. Subsequently, the temperature dependence of the steady state emission spectra and of the time resolved fluorescence decays will be analyzed to determine the energy differences and barriers on the excited state surface. These results, in conjunction with the previously discussed zwitterionic nature of the $^1p^*$ state, enable construction of qualitative and quantitative explanations for most aspects of the photophysics accompanying the photoisomerization of **1**.

II. Experimental Section

Steady state fluorescence spectra were recorded on a SPEX F111XI fluorimeter system using a right angle collection geometry. Excitation and emission band-passes were 1 and 6 nm, respectively. The excitation wavelength was 317 nm. A Hoya L37 long pass filter was inserted in the detection path to prevent scattering and Raman signals from being detected at wavelengths corresponding to second-order diffraction from the monochromator. All solvents were distilled from either Na or CaH_2 immediately prior to use, had optical densities less than 0.02 at 317 nm, and did not generate significant emission signals upon irradiation. The optical density of solutions containing **1**–**4** were 0.5 at 317 nm.[14]

Temperature control for spectra recorded between 250 and 333 K was achieved by insertion of a 1 cm × 1 cm quartz cuvette in an aluminum block through which methanol/2-propanol solution was passed. The temperature of the alcohol solution was controlled using a modified NESLAB LT-50 low-temperature circulating bath. The temperature of the sample was monitored using a Digi-Sense thermometer (Cole-Parmer Model No. 8528–20) and a T-type thermocouple probe that was mounted through a Teflon cap and immersed in the solution to within 0.5 cm of the irradiated region. The sample temperature was maintained to within 0.5 K following thermal equilibration. Temperature control for spectra recorded between 197 and 333 K was achieved by immersing a cylindrical quartz tube in a quartz optical dewar containing methanol. The methanol temperature was adjusted by the addition of aliquots of dry ice. The temperature control was ±1.5 K at the lowest temperatures and ±2.5 K at the highest temperatures studied. Spectra recorded using the two temperature control techniques, at any specific temperature between 250 and 333 K, were indistinguishable.

Nanosecond time resolved fluorescence decays[15] and picosecond optical calorimetry (POC) waveforms[8] were recorded as previously described. Picosecond time resolved fluorescence decays were obtained using the time-correlated single photon counting technique.[16] Specific features of the apparatus used here have been reported.[17] The shortest lifetime accurately resolvable on the nanosecond fluorescence apparatus is 0.8 ns.[18] The fluorescence and POC data sets were fit by minimizing the sum of the squared residuals using a variation of the Levenberg–Marquardt method.[19] More complete discussions of the POC model[20] and fitting methods[21] have been presented.

III. Results

A. Steady State Emission Spectra. Emission spectra from **1**, **2**, and **4** in MCH were measured between 380 and 700 nm

(10) Schuddeboom, W.; Jonker, S. A.; Warman, J. M.; de Haas, M. P.; Vermeulen, M. J. W.; Jager, W. F.; de Lange, B.; Feringa, B. L.; Fessenden, R. W. *J. Am. Chem. Soc.* **1993**, *115*, 3290.
(11) Ma, J.; Zimmt, M. B. *J. Am. Chem. Soc.* **1992**, *114*, 9723.
(12) Tahara, T.; Hamaguchi, H.-O. *Chem. Phys. Lett.* **1994**, *217*, 369.
(13) Sun, Y.-P.; Bunker, C. E. *J. Am. Chem. Soc.* **1994**, *116*, 2430.
(14) The large Stokes shift in these systems minimizes spectral overlap and reabsorption, enabling use of samples with large optical densities.
(15) Zeng, Y.; Zimmt, M. B. *J. Phys. Chem.* **1992**, *96*, 8395.
(16) O'Connor, D. V.; Phillips, D. *Time Correlated Single Photon Counting*; Academic Press: New York, 1984.
(17) Zeglinski, D. M.; Waldeck, D. H. *J. Phys. Chem.* **1988**, *92*, 692.
(18) The instrument response function has a full width at half maximum of 0.9 ns and a full width at one eighth maximum of 2.1 ns.
(19) Press, W. H.; Flannery, B. P.; Teukolsky, S. A.; Vetterling, W. T. *Numerical Recipes*; Cambridge University Press: Cambridge, 1988; Chapter 10.
(20) Ma, J. Ph.D. Thesis, Brown University, 1994.
(21) Morais, J. M.; Zimmt, M. B. Submitted for publication.

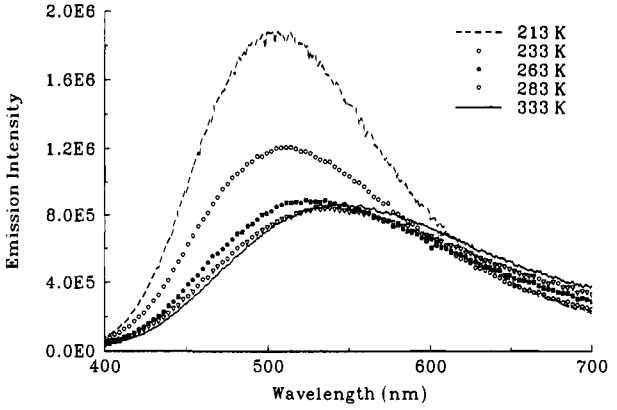

Figure 1. The steady state emission spectrum from **1** in MCH is shown for temperatures between 213 and 333 K. The spectra have been corrected for the monochromator and detector wavelength dependences but have not been corrected for the change in chromophore density with temperature. The emission spectrum at 198 K, which has a peak intensity that is 1.5 times larger than that of the 213 K spectrum, has been omitted in order to assist visualization of the temperature dependent, emission spectral changes at wavelengths longer than 600 nm.

at temperatures ranging from 199 to 333 K. The spectral intensities were corrected for the change in chromophore concentration with sample temperature.[22] The emission quantum yield of **1** between 420 and 700 nm was determined to be 2.02×10^{-3} at 294 K by comparison to the emission from an identical optical density solution of azulene in MCH.[23] The emission quantum yield between 420 and 700 nm at every other temperature T was calculated as the product of (a) the ratio of the integrated areas in the fluorescence spectra, between 420 and 700 nm (area(T)/area(294)) and (b) the emission quantum yield determined at 294 K. The calculation of the **total** emission quantum yield will be described in Section IV following determination of the excited vertical and relaxed conformation emission spectra.

The emission spectra of **1** and **4** at 199 K exhibited a single broad peak centered at 503 and 513 nm, respectively. As the temperature was increased, the intensity of the maximum decreased and the position of the maximum shifted to longer wavelengths (Figure 1 shows this behavior for **1**). For wavelengths longer than 610 nm, the emission intensity from **1** increased at temperatures above 223 K; for **4**, the emission intensity at wavelengths longer than 650 nm increased slightly as the temperature was raised from 243 to 333 K. The emission spectrum from **2** exhibited a maximum at 493 nm and the emission intensity decreased monotonically from 202 to 323 K, with no concomitant shift in the emission maximum.

Figure 2 displays the room temperature, steady state emission spectra from identical optical density solutions of **1** and **2** in various solvents. The line shapes, the intensities, and the line positions are clearly affected by both solvent polarity and viscosity. These steady state spectra will be discussed after the emission spectra of the individual components, the vertical and relaxed conformations, are extracted. The separation of these spectral components is described below.

(22) The optical density at each temperature was calculated using the temperature dependence of the solvent density. For a given sample temperature, the fluorescence intensity at each wavelength was divided by a correction factor obtained from a regression plot of fluorescence signal versus optical density of **1** at room temperature in MCH. No attempt was made to correct for the temperature dependent collection efficiency resulting from the variation of the solvent refractive index.

(23) The quantum yield of azulene in cyclohexane is reported to be 0.024. Berlman, I. B. *Handbook of Fluorescence Spectra of Aromatic Molecules*; Academic Press: New York, 1965; p viii.

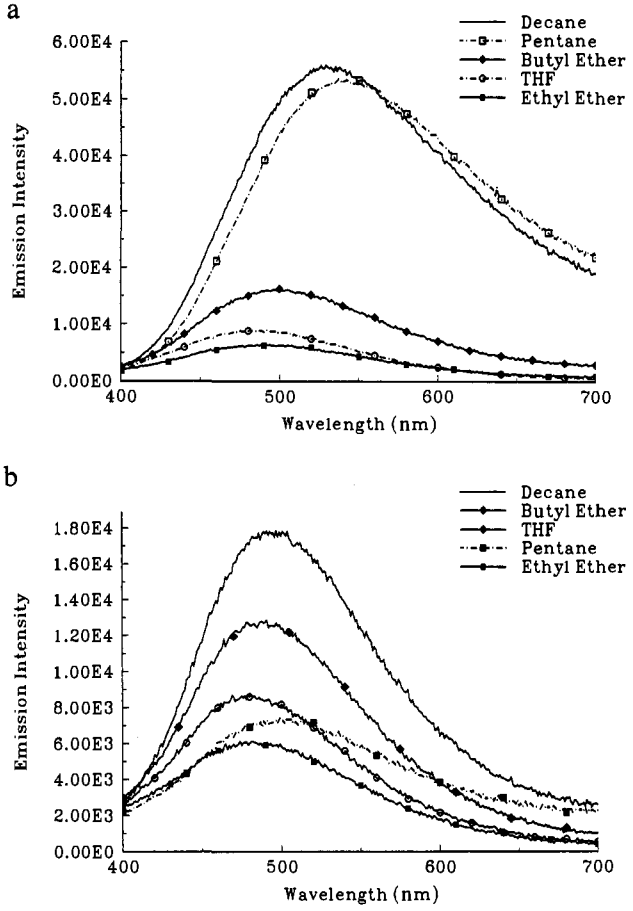

Figure 2. Room temperature emission spectra from **1** (a) and **2** (b) in various solvents. The optical density of each sample was 0.5 at the excitation wavelength of 317 nm. The intensity units are arbitrary. However, the relative intensities of any two spectra in both panels are accurately represented by the indicated intensity scales.

B. Time Resolved Fluorescence Spectra at 294 K. Time resolved fluorescence decays from **1** were determined at 10 nm intervals from 400 to 700 nm using the nanosecond time resolved apparatus.[24] The decays at each wavelength were comprised of two components. The faster decaying component (prompt emission) followed the instrumental response. The second, longer lived component (delayed emission) decayed within 10 ns. The prompt emission dominated the decay profiles obtained at wavelengths shorter than 450 nm, whereas decays detected at wavelengths longer than 650 nm consisted, primarily, of the delayed emission. As a consequence, the time resolved emission spectrum[25] exhibited a bathochromic shift with increasing delay (Figure 3).

The time resolved fluorescence decays at each wavelength were fit to a model with two terms and three variable parameters. The first term was the instrumental impulse response function, scaled by an amplitude parameter. The second term was an exponential decay, with the excited state lifetime as a variable parameter, which was convolved with the instrumental impulse response and scaled by a second amplitude parameter. The fitting results indicated that the delayed emission lifetime was constant, 1.6 ± 0.2 ns, within experimental uncertainty at all wavelengths. The ratio of the number of photons emitted during

(24) The emission bandpass was nominally 7 nm.

(25) Time resolved emission spectra were obtained by scaling the decay curve at each wavelength such that its integral was proportional to the corresponding steady state emission intensity. The scaled intensities, as a function of wavelength at a particular time, comprise the emission spectrum at that delay. The spectra in the figures were obtained by averaging the time resolved spectra over 0.5 ns intervals centered at the stated decay time.

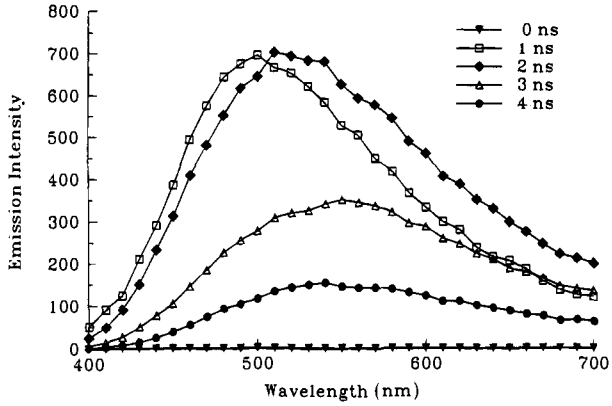

Figure 3. Time dependent emission spectra are shown for **1** in MCH at 294 K. The spectra have been averaged over a 0.5 ns window centered at the indicated decay time. See the Experimental Section and ref 25 for details of how the spectra were constructed.

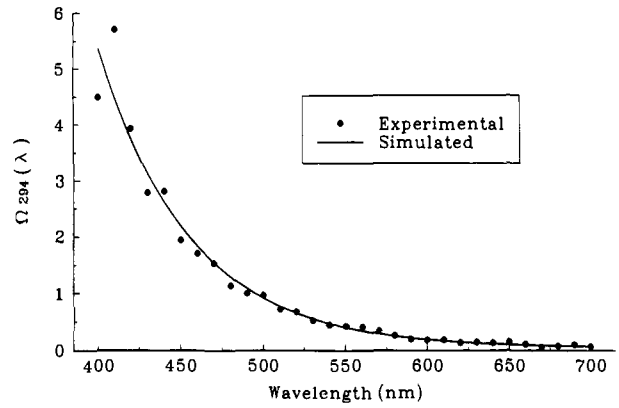

Figure 4. This plot shows the ratio of the number of photons emitted during the prompt emission to the number emitted during the delayed emission as a function of wavelength for **1** in MCH at 294 K. The experimental points are at 10 nm intervals from 400 to 700 nm. The solid line is a fit to the data using the functional form $A + B \exp(C + D\lambda)$. The choice of this function is arbitrary. At 700 nm, the value of this function is 0.0659, whereas the experimental value is 0.0647.

the prompt emission to the number emitted during the delayed emission, $\Omega_{294}(\lambda)$, was calculated at each wavelength from the integrals of the first and second fitting terms between 0 and 20 ns. Figure 4 shows a plot of this ratio, $\Omega_{294}(\lambda)$, as a function of wavelength.

The time resolved emissions of **4** and **2** were also studied. The emission decays from **4** exhibited a similar wavelength dependence as those from **1**, although the relative contribution of the prompt emission was slightly larger for **4** at all wavelengths. The lifetime of the long lived component was 1.3 ± 0.3 ns and was independent of wavelength.[26] The emission decays from **2** at all wavelengths were too fast to resolve with the nanosecond apparatus. Picosecond time resolved, single photon counting experiments, performed in the laboratory of Professor Weber at Brown, exhibited two decay components. As for **1** and **4**, the kinetics of the prompt emission could not be resolved. The delayed emission decayed with a lifetime of 0.45 ns. It was not possible to accurately determine the ratio of the fast to slow emission yields across the fluorescence spectrum due to the small emission quantum yield and the predominant contribution of the fast component at all wavelengths shorter than 600 nm.

C. Temperature Dependence of the Emission Decays from 1 at 700 nm. Time resolved fluorescence decays from **1** in MCH at 700 nm were measured, at temperatures between 253 and 333 K, using the picosecond time resolved, single photon counting apparatus at Pittsburgh. The data were analyzed using a four-parameter, biexponential model, and included convolution with the instrument response function. The ratio of the areas of the fast and slow components for **1** at 700 nm provides the ratio of the prompt to delayed emission quantum yield as a function of temperature, $\Omega_T(700)$ (Table 1). The ^{1}p* decay rate constant was observed to increase with increasing temperature. An Arrhenius analysis of the temperature dependence yielded ln A = 21.1 ± 0.2 and E_a = 0.47 ± 0.06 kcal/mol.

D. Picosecond Optical Calorimetry Studies of 2 and 4. Picosecond optical calorimetry waveforms were collected for **2** and **4** (see Figure 5) in the linear alkane solvents, from pentane through decane, in the manner previously described for **1**.[8] The experimental quantity f is the ratio of (1) the total volume change[27] produced during the decay of the twisted state to (2) the volume change produced by thermalization of the photon energy. This ratio is related to the molar enthalpy change

Table 1. Temperature Dependences of the ^{1}p* Decay Rate Constant and of the Ratio of Prompt to Delayed Emission Quantum Yield at 700 nm for **1** in MCH

temp (K)	τ^1p* (ns)[a]	$\Omega_T(700)$
253	1.67	0.125 ± 0.016
273	1.56	0.062 ± 0.007
293	1.51	0.032 ± 0.003
313	1.43	0.015 ± 0.002
333	1.33	0.001 ± 0.002

[a] The uncertainties are ±0.08 ns.

$\Delta H(^1\text{p}^* \rightarrow S_0)$ and to the partial molar volume change $\Delta V(^1\text{p}^* \rightarrow S_0)$, between the twisted excited state and the ground state, as[8]

$$L_0 h\nu f = \Delta H(^1\text{p}^* \rightarrow S_0) + \Delta V(^1\text{p}^* \rightarrow S_0)/X_S \qquad (1)$$

where L_0 is Avogadro's number, $h\nu$ is the excitation photon energy, and X_S is the thermal expansivity of the solvent. Hence, a plot of $L_0 h\nu f$ versus $1/X_S$ provides $\Delta H(^1\text{p}^* \rightarrow S_0)$ from the intercept and $\Delta V(^1\text{p}^* \rightarrow S_0)$ from the slope. In these studies, X_S is varied by changing the solvent from pentane to decane. From such plots for **2** (see the insert in Figure 5a) and **4**, the twisted state energies in the alkane solvents are 63.3 ± 1.8 and 67 ± 5 kcal/mol, respectively.[28] The partial molar volumes of the twisted excited states of **2** and **4** are 20 ± 6 and 17 ± 20 mL/mol *smaller* than the volumes of the corresponding planar ground states, respectively. The twisted state decay rate constants for **1**–**4** in a variety of solvents, determined using picosecond optical calorimetry, are listed in Table 2.

The large uncertainties in ΔH and ΔV for **4** arise from the failure of the fitting model to accurately simulate the POC waveforms generated in alkanes more viscous than hexane (see the insert in Figure 5b). The large peak at t = 0 cannot be simulated without including absorptive and dispersive contributions from either the vertical or relaxed states prior to equilibration of the relaxed and twisted excited states. The POC data from **4** are more accurately fit using models that incorporate

(26) The similarity of the instrument response function and the long component lifetime (1.3 ns) lead to a larger uncertainty in the ratio of the prompt to delayed emission quantum yields.

(27) The total volume change for each reaction step is equal to ΔH_{RXN}, the molar enthalpy of reaction, multiplied by the solvent thermal expansivity X_S added to ΔV_{RXN}, the partial molar volume change for the reaction. See refs 20 and 21 for more thorough discussions of the calorimetry signal.

(28) The twisted, excited state energy and partial molar volume of **1** were previously determined to be 67.0 ± 1.3 kcal/mol higher and 29 ± 7 mL/mol smaller, respectively, than the comparable quantities for the planar ground state.[8]

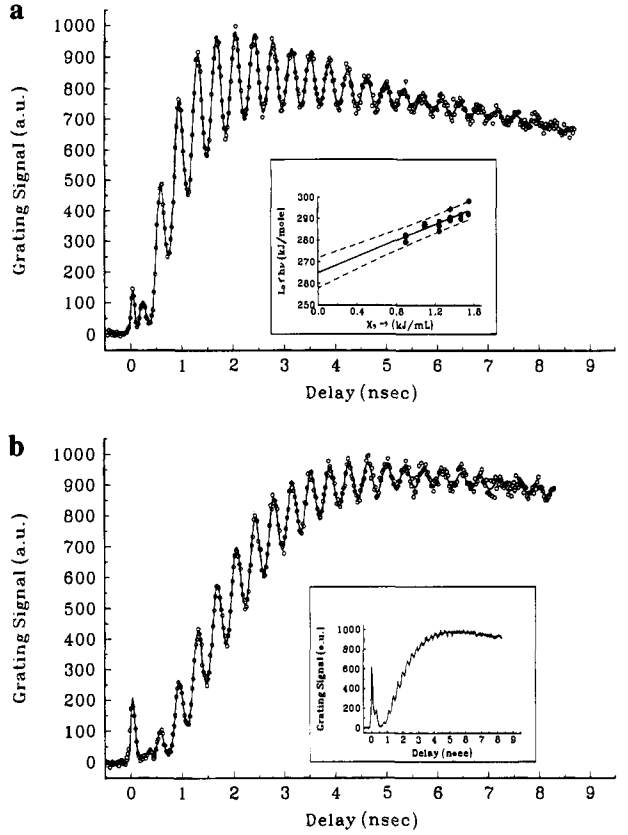

Figure 5. Time dependent POC signals are shown for **2** (a) and for **4** (b) in pentane at 294 K. Every eighth data point is indicated by a circle in the figures. The solid line is a best fit to the data. See refs 20 and 21 for more complete discussions of the data fitting. The inset of (a) shows a plot of L_0hvf versus X_S^{-1} for **2** in the linear alkanes from pentane to decane. The solid line is the linear regression best fit and the dashed lines indicate 90% confidence levels from the linear regression analysis. The intercept is 63.3 kcal/mol (264.8 kJ/mol) and the slope is 20 mL/mol. The inset to (b) shows the POC signal from **4** in decane at 294 K. It was not possible to obtain fits, which accurately simulated the large peak near $t = 0$ and the remainder of the waveform, without inclusion of additional parameters (see text).

Table 2. $^1p^*$ Decay Rate Constants[a] (10^9 s^{-1}) Determined Using POC

solvent	1	2	3	4
n-pentane	0.60	1.85	0.82	0.81
n-decane	0.65	2.0	0.83	0.85
ethyl ether	3.7	12		
THF	11	40		

[a] Uncertainties are less than ±10%.

finite lifetimes and, hence, contributions to the grating signal from the "prompt decay" of the vertical and relaxed states. However, insufficient independent information exists to check the accuracy of the decay rate constants and dispersive and absorptive contributions obtained from these fits. Fortunately, these states decay sufficiently rapidly in pentane that their contributions to the grating signal can be ignored in the fitting procedure.[29] As an alternative, an estimate of $\Delta H(^1p^* \rightarrow S_0)$ for **4** in pentane[30] can be obtained using the experimental value of $f = 0.795 \pm 0.012$, $L_0hv = 90.2$ kcal/mol and reasonable values of $\Delta V(^1p^* \rightarrow S_0)$. The value of $\Delta V(^1p^* \rightarrow S_0)$ for **4** was estimated in three ways: (i) the experimental value for **1** was used (29 mL/mol), (ii) the experimental value for the *p*-methyl derivative **2** was used (20 mL/mol), and (iii) an estimate of $\Delta V(^1p^* \rightarrow S_0) = 11$ mL/mol for **4** was obtained with the assumption that an additional two *p*-methyl groups have the same effect on the volume of reaction as the first pair of *p*-methyl groups. With these estimates of $\Delta V(^1p^* \rightarrow S_0)$, $\Delta H(^1p^* \rightarrow S_0)$ for **4** in pentane is 67.4 ± 3.0 kcal/mol.

IV. Analysis

A. Excited State Emission Spectra from the Vertical and Relaxed Conformations. The photophysics of the TPE derivatives **1**–**4** will be discussed in terms of Scheme 1. In this scheme, the vertical excited state conformation, ^1V, is produced by photon absorption and decays by a combination of fluorescence and an extremely rapid, structural relaxation to form a conformationally relaxed, excited state, ^1R, of unknown geometry. This relaxed excited state also decays by fluorescence and by a fast, structural relaxation process to form the twisted excited singlet state, $^1p^*$. The twisted excited state does not emit in the 400–700 nm region. The $^1p^*$ state is depopulated by two pathways: (i) irreversible, non-radiative internal conversion to form the twisted ground state, ^1p, and (ii) reformation of the conformationally relaxed excited state, ^1R. This set of interconversions leads to significant temperature dependences of the ^1V and ^1R emissions quantum yields. As the maxima and widths of the vertical and relaxed state emission spectra are rather distinct (vide infra), the experimental emission line shape is strongly temperature, viscosity, and solvent polarity dependent.[5,31]

The steady state and time resolved fluorescence data may be used to determine the line shapes of the vertical and the conformationally relaxed excited states emission spectra. The analysis (see Appendix A) is based on the model in Scheme 1 and the following assumptions. First, the prompt emission observed in the time resolved decays is comprised of fluorescence from both the vertical and relaxed excited states, prior to equilibration of the ^1R and $^1p^*$ states, whereas the delayed emission is comprised of fluorescence solely from the relaxed excited state subsequent to equilibration of the ^1R and $^1p^*$ states. Second, the prompt and delayed emissions from the ^1R state are characterized by identical radiative rate constants and emission line shapes. Last, only the ^1R state emission spectrum extends to wavelengths longer than 690 nm. With these assumptions, *the ratio of the photons from the prompt emission to those from the delayed emissions at 700 nm, $\Omega_{294}(700)$, is identical to the ratio of the prompt ^1R emission to the delayed ^1R emission contribution in the steady state emission spectrum at all wavelengths.* Thus, the contributions of the ^1V and ^1R emissions[32] to the steady state emission spectra at 294 K are given by (see eqs A16–19 in Appendix A)

$$I_{Vert,SS}(\lambda) = I_{SS,294}(\lambda)(\Omega_{294}(\lambda) - \Omega_{294}(700))/(\Omega_{294}(\lambda) + 1)$$

$$I_{Rel,SS}(\lambda) = I_{SS,294}(\lambda)(\Omega_{294}(700) + 1)/(\Omega_{294}(\lambda) + 1)$$

where $I_{SS,294}(\lambda)$ is the steady state emission spectrum obtained from **1** in MCH at 294 K and $\Omega_{294}(\lambda)$ was obtained from a fit to the experimental data at 10 nm intervals (the solid line in Figure 4). The calculated ^1V and ^1R emission spectra (see Figure 6) exhibit maxima at 498 and 562 nm, respectively. The

(29) A similar situation apparently holds for **1** and **2** in all alkanes. These olefins may twist by rotating one diphenylmethyl group through the solvent, resulting in less viscous drag. This explanation receives partial support from the larger contribution of prompt emission in **4** compared to **1**.

(30) In pentane, the experimental value of *f* has the smallest contribution from $\Delta V(^1p^* \rightarrow S_0)$.

(31) (a) Stegemeyer, H. *Ber. Bunsenges. Phys. Chem.* **1968**, *72*, 335. (b) Klingenberg, H. H.; Lippert, E.; Rapp, W. *Chem. Phys. Lett.* **1973**, *18*, 417.

(32) This analysis is performed on data between 420 and 700 nm. The data at 400 and 410 nm were not used in an attempt to minimize fluorescence contributions from minor amounts of the cyclization products.

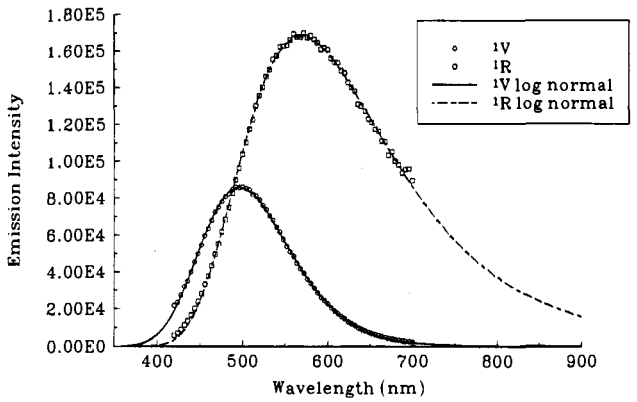

Figure 6. Emission spectra from the excited ^1V and ^1R conformations of **1** at 294 K in MCH are shown. The points were determined from the steady state and time resolved emissions as described in the text. The lines are log-normal fits to the spectra in the range from 420 to 700 nm.

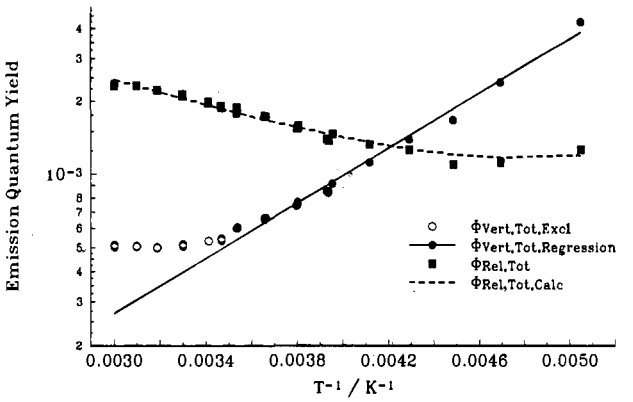

Figure 7. This figure shows the temperature dependent fluorescent quantum yields of the ^1V and ^1R conformations from **1** in MCH. The filled circles were used for the linear regression determination (solid line) of $E_a(^1V \rightarrow ^1R)$. The unshaded circles were excluded from the analysis (see discussion in the text). The dashed line is the best fit to the total (prompt + delayed) emission quantum yield from the excited ^1R conformation.

shape and maximum of the latter spectrum is in acceptable agreement with the time resolved emission spectra observed after 2 ns (see Figure 3).

The ^1V and ^1R emission spectra were converted to wavenumber units and fit to a log normal line shape function.[33] Following reconversion of the log normal fits to nanometer units (Figure 6), the spectra were integrated between 420 and 700 nm and between 300 and 2000 nm.[34] The ratio of these areas was used to estimate the percentage of the ^1V and ^1R emission spectra contained between 420 and 700 nm. For the ^1V and ^1R emissions, these percentages are 98.8 and 75.5, respectively. These percentages are used to obtain the total emission quantum yield (vide infra).

B. Vertical and Relaxed State Emission Quantum Yields. The corrected steady state emission spectra (420−700 nm) from **1** in MCH, at temperatures from 199 to 333 K, were fit as linear combinations of $I_{Vert,SS}(\lambda)$ and $I_{Rel,SS}(\lambda)$ determined in section IV.A. The ratio of the area contributed by the ^1V emission to the area of the experimental spectrum is the fraction of the experimental quantum yield attributable to the ^1V emission, $h_V(T)$. The ^1V state **total emission quantum yield**,[35] $\Phi_{Vert,Tot}$, at each temperature was calculated as the product of $h_V(T)$ and the observed (420−700 nm) emission quantum yield, divided by 0.988. Similarly, the ^1R state **total emission quantum yield**, $\Phi_{Rel,Tot}$, at each temperature was calculated as the product of $(1 - h_V(T))$ and the observed (420−700 nm) emission quantum yield, divided by 0.755. These quantum yields are plotted as a function of temperature in Figure 7.

According to the kinetic model in Appendix A, the temperature dependent, ^1V emission quantum yield is equal to $k_{f,V}/(k_1 + k_{f,V})$ (see Scheme 1 and eq A-12). In order to analyze these data, a value of $A_1 = 2 \times 10^{13}$ s^{-1} was assumed and the weak temperature dependence of the radiative rate constant, $k_{f,V}$, was ignored.[36] The best fit to the ^1V quantum yield data from 213 to 283 K (see Discussion section) gave an activation barrier, $E_a(^1V \rightarrow ^1R)$, for the $^1V \rightarrow ^1R$ interconversion of 2.6 ± 0.4 kcal/mol and $k_{f,V} = 1.7 \times 10^8$ s^{-1}. This fit is indicated by the solid line in Figure 7. Changing the assumed value for A_1 from 0.5 to 10 × 10^{13} s^{-1} had no effect on $E_a(^1V \rightarrow ^1R)$. In contrast, $k_{f,V}$ varied such that $A_1/k_{f,V}$ remained equal to 1.2 × 10^5.

The temperature dependence of the ^1R emission quantum yield is given by eq A-12′ in Appendix A. Using similar assumptions as for the ^1V analysis, *i.e.* $A_1 = A_2 = 2 \times 10^{13}$ s^{-1}, and a temperature independent ^1R radiative rate constant, $k_{f,R}$, the best fit of $\Phi_{Rel,Tot}$ required $E_a(^1R \rightarrow ^1p^*) = 2.4$ kcal/mol, $\Delta E(^1R \rightarrow ^1p^*) = -1.76$ kcal/mol, and $k_{f,R} = 2.56 \times 10^7$ s^{-1}. The dashed line in Figure 7 shows this fit. For values of A_1 and A_2 ranging, independently, from 0.5 to 10 × 10^{13} s^{-1}, $E_a(^1R \rightarrow ^1p^*)$ varied from 2.0 to 4.0 kcal/mol, ΔE varied from −1.6 to −1.9 kcal/mol, and $k_{f,R}$ varied from 2.2 to 2.7 × 10^7 s^{-1}. The rationale for the selection of $A_1 = A_2 = 2 \times 10^{13}$ s^{-1} is presented in the next section.

C. Relaxed State Prompt and Delayed Fluorescence Quantum Yields. There are two contributions to the ^1R state emission quantum yield from **1** in alkane solvents. Following its formation from ^1V, the ^1R state undergoes fluorescence in competition with the formation of $^1p^*$, providing the "prompt" contribution to the relaxed state emission quantum yield. The formation of $^1p^*$ from ^1R is not irreversible, however, and equilibrium is established between the ^1R and $^1p^*$ states in a time that is short $(k_2 + k_{-2})^{-1}$ compared to the overall, excited state decay time $(\sim k_d^{-1})$ of the equilibrium ensemble. Fluorescence from the ^1R state during the decay of the equilibrium ensemble contributes the "delayed" component of the relaxed state emission quantum yield. The prompt and delayed ^1R emission quantum yields may be determined (between 253 and 333 K) from the values of $\Phi_{Rel,Tot}$ and $\Omega_T(700)$ listed in Table 1. These values are plotted versus $1/T$ in Figure 8. Using the activation and energy parameters, as determined from the temperature dependence of the total relaxed state emission quantum yield, and the kinetic model (eqs A-17 and A-18), one can predict the temperature dependences of the prompt and delayed ^1R emission quantum yields. These dependences are also plotted in Figure 8 for the values of the parameters indicated in the figure caption. The value of 2 × 10^{13} s^{-1} assumed for A_1 and A_2 in the previous section yielded values of $E_a(R \rightarrow ^1p^*)$, $\Delta E(R \rightarrow ^1p^*)$, and $k_{f,R}$ that generated the best fits to the temperature dependences of the total ^1R state emission quantum yield and to the prompt and delayed ^1R state emission quantum yields. The value of A_1 also yielded a value of $k_{f,V}$ that was in agreement with previous estimates.[4,37]

(33) The line shape was corrected by multiplication with λ^2 when converted from nm to cm^{-1} units and by λ^{-2} when converted from cm^{-1} to nm units.

(34) Integrations were performed in nm units as the spectrometer is designed to yield photons per unit nm.

(35) The total emission quantum yield includes contributions to the quantum yield from emission outside the 420−700 nm region.

(36) Olmsted, J., III *Chem. Phys. Lett.* **1976**, *38*, 287.

(37) Shultz, D. A.; Fox, M. A. *J. Am. Chem. Soc.* **1989**, *111*, 6311.

V. Discussion

A. Potential Energy Surface for the Photophysics of 1. The results described above provide a rudimentary picture of the potential energy surface upon which the photoisomerization of **1** proceeds. The energies of the three excited state intermediates, ^{1}V, ^{1}R, and ^{1}p*, and the barriers to their interconversions have been determined. Analysis of the absorption and emission spectra indicates that the vertical state (^{1}V) lies 76−77 kcal/mol above the ground state. The energy of ^{1}V does not vary significantly with solvent polarity. The dominant decay channel for the ^{1}V state involves a conformational change which leads to a structurally relaxed, emissive conformation of the excited state, ^{1}R. The barrier to this structural change, 2.6 ± 0.4 kcal/mol, lies between the barriers found to impede the decays of the vertical excited states of *cis*- and *trans*-stilbene.[2] According to the analysis presented above, the rate determining step for the formation of ^{1}p* in fluid solution is the conversion of ^{1}V to ^{1}R. The predicted rate constant for this process at 295 K, 2.4 × 10^{11} s^{-1}, is in good agreement with fluorescence decay rate constants reported by Barbara[4] and transient absorption dynamics reported by Green.[6]

In point of fact, the data presented above provide no direct evidence that the ^{1}V state lies in a potential minimum. As suggested by Barbara et al.,[4] the conformational change that converts ^{1}V into ^{1}R may be impeded more by solvent viscosity than by an internal barrier. By analogy to observations from recent studies of solvation dynamics,[38] one would expect to observe a time dependence of the ^{1}V line shape during an intrinsically barrierless, continuous relaxation. In contrast, Barbara et al.[3] reported comparable decay and appearance kinetics for the blue (^{1}V) and red (^{1}R) emissions, respectively, from **1** but did not report a wavelength dependence of the kinetics.[39] Thus, their results are consistent with the involvement of a kinetically significant ^{1}V intermediate. The successful disection of the temperature dependent emission spectra (199−333 K) of **1** in terms of two species with temperature independent line shapes provides additional evidence that the ^{1}V state possesses unique kinetic and spectroscopic properties.

It must be noted that the Arrhenius plot of the ^{1}V emission quantum yield (Figure 7) exhibits considerable curvature at temperatures above 283 K. This curvature could be interpreted as indicating thermal repopulation of the ^{1}V state from ^{1}R. Based on the estimated difference in the ^{1}V and ^{1}R energies, the ^{1}V emission quantum yield should increase by less than 10^{-6} when thermal repopulation is included in the analysis—much less than the observed increase. As an alternative explanation, the apparent increase of the ^{1}V quantum yields at higher temperatures may be an artifact of assuming temperature independent line shapes for the ^{1}V and ^{1}R emissions. For example, thermally induced broadening on the blue edge of the ^{1}R line shape would be interpreted, in our analysis, as an additional source of ^{1}V emission. Pursuing this further, the ^{1}V emission quantum yield is at least four times smaller than that from ^{1}R in this temperature range. Furthermore, the ^{1}R emission quantum yield is increasing as the temperature increases. Thus, the magnitude of the ^{1}R emission intensity misassigned to ^{1}V emission would increase at higher temperatures. Improper attribution of a small portion of the ^{1}R emission to emission from ^{1}V would produce upward curvature in the quantum yield plot of the latter and a value of $E_a(^1V \rightarrow {}^1R)$ which is too small. Support for this explanation is found in the slight downward curvature observed in $\Phi_{Rel,Tot}$ in Figure 7 in the same temperature range where $\Phi_{Vert,Tot}$ exhibits the upward curvature. The misassignment of the emission is less noticeable in $\Phi_{Rel,Tot}$ as this quantity is nearly an order of magnitude larger. Clearly, the value of 2.6 kcal/mol obtained from the ^{1}V emission quantum at lower temperatures may be considered a lower limit to the ^{1}V→^{1}R barrier. The impact of a small line shape error on the interpretation of the ^{1}R dynamics should be less significant for the reason noted above.

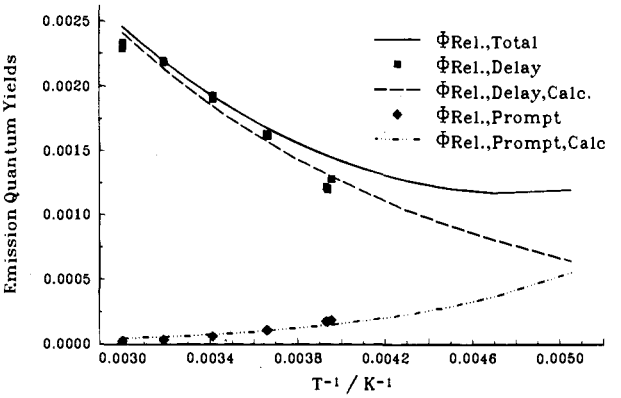

Figure 8. The temperature dependence of the fluorescence quantum yields is plotted for the total, prompt, and delayed ^{1}R emission from **1** in MCH. The solid line is the best fit to the total ^{1}R emission quantum yield (also displayed in Figure 7). The dashed and dot-dash lines are the delayed and prompt ^{1}R emission quantum yields, respectively, predicted using $A_1 = A_2 = 2 \times 10^{13}$ s^{-1}, $E_a(^1R \rightarrow {}^1p^*) = 2.4$ kcal/mol, $\Delta E(^1R \rightarrow {}^1p^*) = -1.76$ kcal/mol, and $k_{f,R} = 2.56 \times 10^7$ s^{-1}.

The ^{1}R state decays by both fluorescence and a non-radiative structural relaxation that generates the ^{1}p* state. The latter process is impeded by a barrier of ~2.4 kcal/mol. At 294 K in MCH, the ^{1}R radiative and ^{1}R→^{1}p* formation rate constants are 2.6 × 10^7 and 3.3 × 10^{11} s^{-1}, respectively. In non-polar solvents, the ^{1}R→^{1}p* transformation is reversible. At 294 K, the rate constant of the endothermic ^{1}p*→^{1}R process is 1.6 × 10^{10} s^{-1}. This repopulation of ^{1}R is roughly 30 times faster than the observed ^{1}p* decay rate constant. Thus, the equilibrium mixture, consisting of 5% ^{1}R and 95% ^{1}p* at 294 K, is achieved prior to significant radiationless decay to the ground state from the twisted geometry. During the decay of the equilibrium mixture, the ^{1}R fluorescence quantum yield increases from 8 × 10^{-5}, the "prompt" contribution, to the steady state value of 2 × 10^{-3}. Based on the previously determined value of 67 kcal/mol for the energy of ^{1}p* in alkane solvents[8] and the value of $\Delta E = -1.76$ kcal/mol, determined herein, the ^{1}R state lies ≤69 kcal/mol above the planar ground state and 7−8 kcal/mol below the ^{1}V state. This determination completes a rudimentary description of the barriers and energy differences separating the intermediates in the photoisomerization of **1**.

B. Structural Perturbation of the Photoisomerization PES. The longest wavelength absorption band in **1**−**4** exhibits a solvent independent, bathochromic shift of approximately 4 nm for every two *p*-methyl groups substituted on the phenyls (data not shown). The room temperature emission spectra from **1**, **2**, and **4** in diethyl ether exhibit a similar, 3 nm red shift per pair of substituted *p*-methyl groups.[40] Thus, the ^{1}V state energy decreases by ~0.8 kcal/mol for each pair of *p*-tolyl groups substituted for phenyl groups on the alkene. As it was not

(38) (a) Kosower, E. M.; Huppert, D. *Annu. Rev. Phys. Chem.* **1986**, *37*, 127. (b) Castner, E. W., Jr.; Maroncelli, M.; Fleming, G. R. *J. Chem. Phys.* **1987**, *86*, 1090.

(39) Klingenberg et al.[31b] reported dispersion of the ns decay kinetics for **1** in MCH/isopentane between 86 and 128 K. The dispersion observed is due, in part, to unresolved contributions from both ^{1}V and ^{1}R emissions. Subsequent work by Barbara et al.,[4] with better time resolution, confirms this explanation.

(40) Diethyl ether was used to minimize the contribution of the ^{1}R state to the observed emission spectra. The emission spectrum of **3** contained a sufficient contribution from photoproduct to obscure the trend observed with the other three alkenes.

possible to separate the contributions of the ^1V and ^1R emissions to the steady state fluorescence spectra from alkenes **2**, **3**, and **4**, the energy differences between the ^1R and $^1p^*$ states in these alkenes were not determined. Nearly identical emission maxima were observed from solutions of **1**, **3**, and **4** in pentane at 294 K,[41] thus, it does not appear that the *p*-methyl groups alter the ^1R state energy significantly.

In contrast, the energy, as well as the decay dynamics, of the $^1p^*$ state is strongly affected by the *p*-methyl substitution pattern. As determined by picosecond optical calorimetry, the twisted excited state decay rate constant for **2**, in pentane, is three times larger than for **1**, whereas those for **3** and **4** are only 33% larger than for **1**. The symmetrical substitution of four methyl groups on the para positions of the phenyl rings has no measurable effect on the $^1p^*$ state energies (compare **1** and **4**). Asymmetric substitution of two *p*-methyls, as in **2**, generates a $^1p^*$ state that lies 3−4 kcal/mol lower in energy than the $^1p^*$ state in the symmetrical alkenes, **1** and **4**. The significant decrease in the $^1p^*$ state energy, induced by the subtle asymmetric substitution of two methyl groups for hydrogen, provides further confirmation of Schilling and Hilinski's proposal of zwitterionic character in the twisted excited singlet state of tetraphenylethylene.[7]

The energy of a zwitterionic, twisted state in **1** may be estimated from literature data. Leigh and Arnold[42] determined an activation barrier to thermal isomerization in **1** of 35.5 kcal/mol, thus providing a value of the ^1p state energy. Sim et al. have reported the electrochemical oxidation and reduction potentials of various, substituted benzylic, cumyl, and diphenylmethyl radicals in acetonitrile.[43] The difference in the oxidation and reduction potentials of the diphenylmethyl radical in acetonitrile is 1.49 eV (34.4 kcal/mol). Thus, a hypothetical, zwitterionic, twisted state, in which the cationic and anionic centers are fully solvated by acetonitrile and in which there is zero Coulombic interaction energy between the anionic and cationic termini, lies 70 kcal/mol above the planar ground state. The energy change attending reduced solvation[44] and increased Coulombic interactions, appropriate to the real zwitterionic twisted state in alkane solvents, is difficult to predict quantitatively. However, the similarity between the above, zeroth-order estimate and the observed twisted excited state energies for **1** in alkane and ether solvents is noteworthy.

The dependence of the zwitterionic $^1p^*$ state energy on the methyl substitution pattern may be understood by reference to the redox potentials of substituted diphenylmethyl radicals. The di-*p*-tolylmethyl radical is 0.11 eV (2.5 kcal/mol) easier to oxidize than the unsubstituted, diphenylmethyl radical.[43] From this difference, the $^1p^*$ state energy in **2** should lie at least 2.5 kcal/mol lower in energy than in **1**, as is experimentally observed.[45] The di-*p*-tolylmethyl radical is 0.11 eV (2.5 kcal/mol) harder to reduce than the unsubstituted, diphenylmethyl radical.[43] Thus, the $^1p^*$ state energy in tetratolylethylene, **4**, should be very similar to that of **1**, which is also experimentally observed.

The lower $^1p^*$ energy in **2** provides a qualitative explanation for the small total and delayed ^1R emission quantum yields observed in alkane solvents. If the ^1R state energy in **2** is similar to those of **1**, **3**, and **4**, then the $^1R-{}^1p^*$ energy gap is ~3 kcal/mol larger in **2** than in the other alkenes. As a consequence, the extent of thermal repopulation from $^1p^*$ to ^1R will be reduced by a factor of 100. Furthermore, the faster $^1p^*$ decay rate constant in **2** reduces the time available for ^1R fluorescence in the equilibrium ensemble, by a factor of 3, as compared to **1**. Thus, the delayed fluorescence quantum yield from **2** is expected to be insignificant (reduced by ~300) relative to that of **1**. Although the experimental emission quantum yield of 4.8×10^{-4} from **2** in MCH at 294 K was not partitioned into vertical and relaxed contributions, this value is 1.7 times smaller than the sum of the ^1V and prompt ^1R emission quantum yields from **1** in MCH at 294 K and it is 5.2 times smaller than the total emission quantum yield from **1**. Clearly, more than the $^1R-{}^1p^*$ equilibration is affected by the di-*p*-methyl substitution. Although extrapolation of the photophysics in **1** to **2** does not quantitatively reproduce the latter's observed quantum yield data, it does generate results that are in qualitative agreement.

C. Solvent Perturbation of the Photoisomerization Dynamics. Solvent properties strongly influence the dynamics and the luminescence properties of **1**−**4**. Most of the changes may be understood by consideration of (i) polarity effects on the decay processes of the $^1p^*$ state and (ii) viscosity effects on the rate constants of interconversion among the three states. For example, increased solvent polarity lowers the $^1p^*$ state energy, increases its non-radiative decay rate constant[7] to ^1p, and increases the barrier to reformation of ^1R, thus reducing the quantum yield of delayed ^1R fluorescence. The activation barrier for the $^1R \rightarrow {}^1p^*$ interconversion may also decrease slightly with increased solvent polarity,[2,46] reducing the prompt ^1R emission quantum yield also. A diminishing contribution of delayed ^1R emission from **1** in the series of solvents pentane, dibutyl ether, and diethyl ether explains the decrease in the total emission quantum yield, the blue shift in the maximum, and the dramatic drop in the emission spectrum at 700 nm (see Figure 2). Similarly, the reduced intensity of the red tail in the emission spectrum from **2** in ether, in comparison to pentane, may be attributed to a drop in the delayed ^1R emission quantum yield. Increased solvent viscosity slows the interconversion among the three excited state species. This slowing increases the ^1V emission quantum yield and reduces the ^1R delayed quantum yield. As the latter is the major source of ^1R emission in alkane solvents, the total ^1R quantum yield is reduced. This effect explains the concomitant increase of the emission intensity in the blue and the decrease of intensity in the red from **1** as the solvent is changed from pentane to decane or from ether to tetrahydrofuran.

One surprising result from the picosecond optical calorimetry studies is that the $^1p^*$ energy of **2** in alkane solvents is lower than the $^1p^*$ energy for **1** in tetrahydrofuran. Schilling and Hilinski[7] reported a linear correlation between the logarithm of **1**'s $^1p^*$ decay rate constant and solvent polarity, which subsequently was quantified in terms of reductions of the $^1p^*-{}^1p$ energy gap.[8] In apparent contradiction to that trend, **2**'s $^1p^*$

(41) For these three compounds, the 294 K emission is dominated by the relaxed state emission. The emission maxima were previously reported.[11]

(42) Leigh, W. J.; Arnold, D. R. *Can. J. Chem.* **1981**, *59*, 609.

(43) Sim, B. A.; Milne, P. H.; Griller, D.; Wayner, D. D. M. *J. Am. Chem. Soc.* **1990**, *112*, 6635.

(44) There are at least two contributions to the difference in solvation energies for the hypothetical twisted excited state and the real one. The first contribution arises because the electrochemistry was performed in acetonitrile and the calorimetry experiments were performed in alkanes. The second arises from decreased solvent access to the principally charged carbons in **1**−**4** (ethylenic) versus the ions (methylene).

(45) (a) Substituents have larger impacts on radical oxidation potentials where ion solvation is minimal, i.e. in the gas phase, in comparison to that in acetonitrile (see Table IV in Sim. et al.[43]). Thus, one can rationalize the observed larger effect of di-*p*-methyl substitution on the $^1p^*$ state energy in alkanes compared to its effect on the oxidation potential measurements in acetonitrile. (b) Leigh and Arnold[42] observed that alkyl and alkoxy substituents and solvent polarity had minimal influence on the barrier to thermal isomerization in substituted tetraarylethylenes. Thus, in analyzing substituent effects on the $^1p^*$ energy, it is reasonable to assume that the ^1p energies of **1** and **2** are equal and solvent independent.

(46) (a) Hicks, J. M.; Vandersall, M. T.; Sitzmann, E. V.; Eisenthal, K. B. *Chem. Phys. Lett.* **1987**, *135*, 413. (b) Tepper, R. J.; Hooper, A. J.; Waldeck, D. H.; Zimmt, M. B. *Chem. Phys. Lett.* **1992**, *191*, 411.

decay rate constant in pentane is six times smaller than **1**'s in THF, whereas, the estimated $^1p^*-^1p$ energy gaps are 28 and 30 kcal/mol, respectively.[45b] The $^1p^*$ non-radiative decay process may be thought of as a charge recombination, electron transfer reaction in the Marcus inverted region.[47] As such, effecting a reduction of the $^1p^*$ energy in **1** by an increase in the solvent polarity simultaneously produces an increase in the solvent reorganization energy, which further accelerates the $^1p^*$ decay process. The *p*-methyl substitution lowers the $^1p^*$ energy in **2** without producing a corresponding increase in the solvent reorganization energy. Thus, one should not expect a single correlation between $^1p^*$ energy and decay rate constant for all solvents and substituted derivatives of **1**. It is worth noting that the percentage increase of the $^1p^*$ decay rate constants from pentane to ether, or from ether to THF, is nearly identical for **1** and **2**.

D. Extensions. The results from this study may shed light on two related issues in the literature. First, Schuddeboom et al.[10] recently provided definitive evidence of a dipole moment in the $^1p^*$ state of **1** in alkane solvents. Using the time resolved microwave conductivity technique, they determined a dipole moment of ≥ 7.5 D for this state. Their results also indicated that the associated dipole orientational relaxation time, estimated to be on the order of 15 ps, did not appear to involve overall rotation of the molecule, as would be expected for a "permanent" dipole. From the present study, the time required for the $^1p^*\rightarrow{}^1R$ interconversion is ~60 ps in MCH. Using this value for the $^1p^*$ lifetime and the rotation times of *trans*-stilbene in hexane or in decane[48] to estimate the rotation time of **1** (*i.e.*, 13 or 32 ps), one expects effective dipole reorientation times of 11−21 ps, which are in reasonable agreement with the reported value.[10] The $^1p^*\rightarrow{}^1R$ process certainly makes an important contribution to the loss of dipole orientational correlation. Given the complexity and associated errors in the present spectral analysis and the possibility of a slightly different dipole relaxation time than previously estimated, the reversibility of the $^1R\rightarrow{}^1p^*$ transformation provides a simple explanation of the microwave conductivity results.

The second issue relates to what additional implications the present study provides regarding the photoisomerization of stilbene and, in particular, the nature of its $^1p^*$ state. Certainly none of the quantitative results regarding the shape of the excited state potential energy surface may be directly transposed to stilbene. However, the similarity of the experimental $^1p^*$ energy in **1** and the value calculated, from the redox potentials and ground state barrier, warrants a similar calculation for stilbene. Accordingly, the thermal barrier to *trans*-stilbene isomerization is 48 kcal/mol and the difference in enthalpy between the trans and cis forms is taken to be 4.6 kcal/mol.[49] Spectroscopic data place the trans excited state at 92 kcal/mol above the ground state trans form[50] and the cis state about 85 kcal/mol above the ground state cis form.[51] The energy of the phantom state, relative to the trans excited state, may now be estimated.

First, consider the case of a zwitterionic phantom state. The difference in the benzyl radical oxidation and reduction potentials is 2.16 eV (49.7 kcal/mol).[43] Thus, a hypothetical, improperly solvated (vide supra) zwitterionic $^1p^*$ state in stilbene lies roughly 98 kcal/mol above the *trans*-stilbene ground state. This energy is about 6 kcal/mol above the S_1 state in *trans*-stilbene. As an endoergic S_1 to $^1p^*$ transformation in stilbene has not received any previous support, the energy correction due to Coulombic and other interactions, not properly accounted for in the simple twist plus redox calculation, would need to exceed 7 kcal/mol in order for a zwitterionic $^1p^*$ state to lie below the S_1 state.

Given the ambiguity of the above comparison, it is appropriate to perform an analogous calculation of the energy of the alternate electronic configuration previously advanced for twisted excited states: a radical−electronically excited radical configuration[52] in the twisted geometry. The lowest energy, electronic excited state of the benzyl radical lies 62 kcal/mol (2.67 eV) above the ground state.[53] This crude calculation places the twisted, radical−excited radical configuration 110 kcal/mol above the *trans*-stilbene ground state, or nearly 20 kcal/mol above the *trans*-stilbene S_1 level.[54] This calculation ignores exchange interactions between the two, degenerate excited configurations. However, exchange stabilization in pyrene excimer, a system with much greater overlap and potential for exchange than the twisted state of stilbene, amounts to less than 10 kcal/mol.[55] It is unlikely that the energy of a radical−excited radical state in stilbene would lie below 100 kcal/mol; apparently eliminating a diradical configuration for the twisted excited state in stilbene.

Interestingly, this leads to another, rather puzzling dilemna. A strong dependence of the $^1p^*$ decay rate constant on the $^1p^*-^1p$ energy gap has been demonstrated for **1** and, indirectly, **2**. Assuming the $^1p^*$ state in stilbene lies a few kilocalories per mole below S_1, the energy gap at the twisted geometry is ~40 kcal/mol for stilbene and 32 kcal/mol for **1**. If the promoting modes for internal conversion are the same for both twisted excited states, then the larger gap in stilbene should lead to a slower radiationless decay rate constant. In contrast, the twisted excited state lifetime[3] in stilbene is less than 150 fs, 10^4 times smaller than in **1**. There are at least two possible explanations for the faster $^1p^*$ radiationless decay rate constant in stilbene. First, the $^1p^*-^1p$ electronic coupling may be much larger in stilbene, indicating significant differences in the $^1p^*$ electronic configurations of stilbene and **1**. Second, the presence of vinylic C−H bonds in stilbene may generate more favorable Franck−Condon factors for internal conversion. Interestingly, the twisted excited state lifetime in 1,1-biindanylidene, a stilbene analog in which the vinylic C−H bonds have been replaced by a relatively stiff 5 C ring, is 10 ps,[56] more than sixty times longer than in stilbene. The difference in decay rate constants cannot be unambiguously attributed to the absence of the vinylic C−H bonds, nor does it lead to stilbene lifetimes comparable to those in **1**. None the less, it does support the idea that Franck−Condon factors could be contributing to the significant difference in the twisted excited state dynamics of stilbene and tetraphenylethylene.

These kinetic and energetic comparisons cannot unambiguously identify the electronic configuration in the twisted excited state of stilbene. It seems clear from the above considerations,

(47) (a) Marcus, R. A. *J. Chem. Phys.* **1956**, *24*, 966. (b) Closs, G. L.; Miller, J. R. *Science* **1988**, *240*, 440. (c) Gould, I. R.; Young, R. H.; Moody, R. E.; Farid, S. *J. Phys. Chem.* **1991**, *95*, 2068.

(48) (a) Kim, S. K.; Fleming, G. R. *J. Phys. Chem.* **1988**, *92*, 2168. (b) Lee, M.; Bain, A. J.; McCarthy, P. J.; Han, C. H.; Haseltine, J. N.; Smith, A. B., III; Hochstrasser, R. M. *J. Chem. Phys.* **1986**, *85*, 4341.

(49) Saltiel, J.; Ganapathy, S.; Werking, C. *J. Phys. Chem.* **1987**, *91*, 2755.

(50) Champagne, B. B.; Pfanstiel, J. F.; Plusquellic, D. F.; Pratt, D. W.; van Herpen, W. M.; Meerts, W. L. *J. Phys. Chem.* **1990**, *94*, 6.

(51) Petek, H.; Fujiwara, Y.; Kim, D.; Yoshihara, K. *J. Am. Chem. Soc.* **1988**, *110*, 6269.

(52) (a) Malrieu, J. P.; Nebot-Gil, I.; Sanchez-Marin, J. *Pure Appl. Chem.* **1984**, *56*, 1241. (b) Nebot-Gil, I.; Malrieu, J.-P. *Chem. Phys. Lett.* **1981**, *84*, 571.

(53) Friedrich, D. M.; Albrecht, A. C. *Chem. Phys.* **1974**, *6*, 366.

(54) A similar calculation for the neutral, twisted excited state energy in **1** yields 90 kcal/mol. The lowest excited state of the diphenylmethyl radical lies at 55 kcal/mol. Bromberg, A.; Schmidt, K. H.; Meisel, D. *J. Am. Chem. Soc.* **1984**, *106*, 3056.

(55) Gilbert, A.; Baggott, J. *Essentials of Molecular Photochemistry*; CRC Press: Boca Raton, 1993; p 155.

(56) Doany, F. E.; Heilweil, E. J.; Moore, R.; Hochstrasser, R. M. *J. Chem. Phys.* **1984**, *80*, 201.

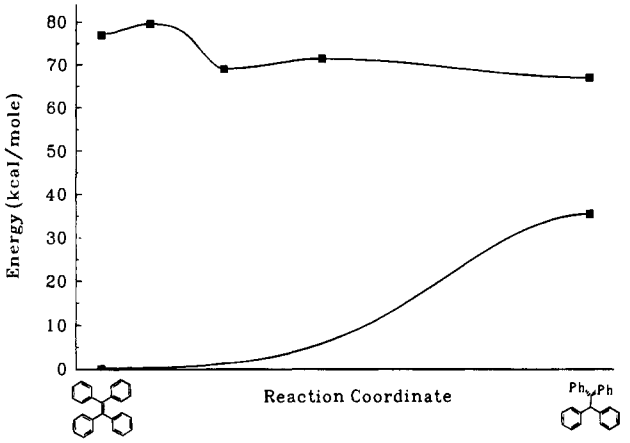

Figure 9. This figure is a model for the ground and first excited potential energy surfaces of **1** along the photoisomerization reaction coordinate. The solid squares indicate experimentally determined energies (see the text for the determination of these quantities). The reaction coordinate involves more extensive structural change than simple twisting about the ethylenic double bond, although the actual structural changes have not been identified.

however, that the phantom state is more likely to be characterized as zwitterionic than as biradical. An additional caveat to this analysis is the failure to consider the role of doubly excited electronic configurations (^{1}p**). The role of such states has been proposed.[57] None the less, the above considerations are useful because they highlight rather significant differences in what appear to be very similar systems (stilbene and **1**) and they underscore the need for additional studies of the potential energy surface in stilbene.

VI. Conclusion

These studies provide a rudimentary map of the singlet, photoisomerization potential energy surface in tetraphenylethylene (Figure 9). The vertical excited state lies 77 kcal/mol above the ground state and is separated from a structurally relaxed, excited conformation by a barrier of 2.6 kcal/mol. The relaxed state energy is 69 kcal/mol. The barrier between the relaxed state and the twisted excited singlet state, the essential intermediate in the photoisomerization reaction, is 2.4 kcal/mol. The twisted excited state energy is sensitive to solvent polarity as well as to structural perturbations, but lies 2 kcal/mol below the relaxed excited state for **1** in alkane solvents.

The involvement of three excited state species along the photoisomerization reaction pathway in **1** leads to interesting, yet interpretable, spectra and dynamics. The POC and fluorescence studies reported here (i) provide additional evidence for the zwitterionic nature of ^{1}p*, originally proposed by Schilling and Hilinski[7], (ii) assist in the development of structure–energy and structure–kinetic correlations for the twisted excited state, and (iii) provide a rudimentary map of the potential energy surface along the photoisomerization coordinate. A number of interesting questions in these systems remain unanswered, including the geometry of the relaxed excited state, the coupling of the photocyclization and photoisomerization pathways, and the absolute dynamics of the ^{1}V decay and the prompt ^{1}R rise and decay. Efforts to address the latter questions are currently in progress.

Acknowledgment. D.H.W. and M.B.Z. thank the National Science Foundation for financial support of this work. Additional support from the NSF-PYI program, the 3M Corporation, and the Camille and Henry Dreyfus Foundation is gratefully acknowledged by M.B.Z. D.H.W. gratefully acknowledges the donors of the Petroleum Research Fund, administered by the American Chemical Society, for partial support of this work. M.B.Z. would like to thank Professor Peter Weber for assistance in determining the fluorescence lifetime of **2**.

(57) Hohlneicher, G.; Dick, B. *J. Photochem.* **1983**, *27*, 115.

Appendix A

A1. Excited State Kinetic Model. For the model in Scheme 1, the rate equations describing the excited state populations are

$$\frac{dn_{v*}(t)}{dt} = -Xn_{v*}(t) \quad \text{(A-1)}$$

$$\frac{dn_{r*}(t)}{dt} = -Yn_{r*}(t) + k_1n_{v*}(t) + k_{-2}n_{p*}(t) \quad \text{(A-2)}$$

$$\frac{dn_{p*}(t)}{dt} = -Zn_{p*}(t) + k_2n_{r*}(t) \quad \text{(A-3)}$$

where $X \equiv k_1 + k_{f,V}$; $Y \equiv k_2 + k_{f,R}$; $Z \equiv k_{-2} + k_d$. $n_{v*}(t)$, $n_{r*}(t)$, and $n_{p*}(t)$ are respectively the time dependent vertical, relaxed, and twisted excited state populations following excitation. For the discussion of quantum yields, the appropriate initial conditions are

$$n_{v*}(0) \equiv 1; \quad n_{r*}(0) = n_{p*}(0) = 0 \quad \text{(A-4)}$$

The time dependent probability of each state being populated is given by

$$n_{v*}(t) = \exp(-Xt) \quad \text{(A-5)}$$

$$n_{r*}(t) = [\alpha \exp(-Xt) + \beta \exp(-\beta_1 t) + \gamma \exp(-\beta_2 t)] \quad \text{(A-6)}$$

$$n_{p*}(t) = [A \exp(-Xt) + B \exp(-\beta_1 t) + \Gamma \exp(-\beta_2 t)] \quad \text{(A-7)}$$

where

$$\alpha = \frac{k_1(Z-X)}{(X-\beta_1)(X-\beta_2)}; \quad \beta = \frac{k_1(\beta_1 - Z)}{(X-\beta_1)(\beta_1-\beta_2)}; \quad \gamma = \frac{k_1(Z-\beta_2)}{(X-\beta_2)(\beta_1-\beta_2)}$$

$$A = \frac{k_1k_2}{(X-\beta_1)(X-\beta_2)}; \quad B = \frac{-k_1k_2}{(X-\beta_1)(\beta_1-\beta_2)}; \quad \Gamma = \frac{k_1k_2}{(X-\beta_2)(\beta_1-\beta_2)}$$

$$\beta_{1,2} = \frac{(Y+Z) \pm [(Y-Z)^2 + 4k_2k_{-2}]^{1/2}}{2}; \quad (\beta_1 > \beta_2) \quad \text{(A-8)}$$

The time and wavelength dependent probability functions for fluorescence from the vertical and relaxed excited states [number of photons emitted/s·nm·photon absorbed] are

$$I_{Vert}(\lambda,t) = g_{V*}(\lambda)[k_{f,V} \exp(-Xt)] \quad \text{(A-9)}$$

$$I_{Rel}(\lambda,t) = g_{R*}(\lambda)\{k_{f,R}[\alpha \exp(-Xt) + \beta \exp(-\beta_1 t) + \gamma \exp(-\beta_2 t)]\} \quad \text{(A-9')}$$

where $g_{V*}(\lambda)$ and $g_{R*}(\lambda)$ [units are nm^{-1}] denote the line shape functions of the vertical and relaxed excited state emissions. The line shape functions are normalized to unity upon integration. Integration in units of nm is appropriate as the fluorimeter output is corrected to give photons per nm.

$$\int_0^\infty g_{V*}(\lambda)\,d\lambda = \int_0^\infty g_{R*}(\lambda)\,d\lambda = 1 \qquad \text{(A-10)}$$

The steady state, wavelength dependent probability functions for fluorescence from the vertical and relaxed states are the time integrals of eqs A-9 and A-9′, respectively.

$$I_{Vert,SS}(\lambda) = \int_0^\infty I_{Vert}(\lambda,t)\,dt \qquad \text{(A-11)}$$

$$I_{Rel,SS}(\lambda) = \int_0^\infty I_{Rel}(\lambda,t)\,dt \qquad \text{(A-11′)}$$

Integration of these probability functions from "0" to "∞" yields the vertical and relaxed state emission quantum yields. Substitution of eqs A-8, A-9, and A-10 into eq A-11 yields the following expressions for the quantum yields:

$$\Phi_{Vert,Tot} = \frac{k_{f,V}}{k_1 + k_{f,V}} \qquad \text{(A-12)}$$

$$\Phi_{Rel,Tot} = \frac{k_1}{k_1 + k_{f,V}} \frac{k_{f,R}(k_{-2} + k_d)}{\beta_1\beta_2} \qquad \text{(A-12′)}$$

The temperature dependence of the vertical and relaxed state quantum yields may be calculated using eqs A-12 and A-12′, provided values for the rate constants and their corresponding activation parameters can be determined. In the next section, the steady state and time-integrated time-resolved fluorescence data will be used to determine the normalized emission spectral shapes, $g_{V*}(\lambda)$ and $g_{R*}(\lambda)$.

A2. Pure Relaxed and Vertical Fluorescence Spectra. The total steady state and wavelength dependent probability function for fluorescence is the sum of the probability functions for both the vertical and relaxed excited states,

$$I_{SS}(\lambda) = \int_0^\infty \{I_{Vert}(\lambda,t) + I_{Rel}(\lambda,t)\}\,dt = I_{Vert,SS}(\lambda) + I_{Rel,SS}(\lambda) \qquad \text{(A-13)}$$

$I_{SS}(\lambda)$ is the line shape of the experimental spectrum. $I_{SS}(\lambda)$ may also be expressed in terms of emission probabilities associated with the prompt (fast) and delayed (slow) decay processes. First, the total wavelength and time dependent probability function for fluorescence, expressed as the sum of these quantities for the vertical and relaxed states, may be grouped according to the associated decay rate constants

$$\begin{aligned} I(\lambda,t) &= IV_{ert}(\lambda,t) + I_{Rel}(\lambda,t) \\ &= \{[g_{V*}(\lambda)k_{f,V} + g_{R*}(\lambda)k_{f,R}\alpha]\exp(-Xt) + \\ &\quad g_{R*}(\lambda)k_{f,R}\beta\exp(-\beta_1 t)\} + (g_{R*}(\lambda)k_{f,R}\gamma\exp(-\beta_2 t)) \\ &= \{I_{fast}(\lambda,t)\} + (I_{slow}(\lambda,t)) \end{aligned} \qquad \text{(A-14)}$$

As the decay constants X and β_1 are both too fast to be resolved, the associated fluorescence probability terms are combined. Thus, the second expression for the total steady state and wavelength dependent probability function for fluorescence is

$$I_{SS}(\lambda) = \int_0^\infty I_{fast}(\lambda,t)\,dt + \int_0^\infty I_{slow}(\lambda,t)\,dt = I_{fast}(\lambda) + I_{slow}(\lambda) \qquad \text{(A-13′)}$$

$\Omega_{294}(\lambda)$ is defined as the probability of fluorescence during the fast decay divided by the probability of fluorescence during the slow decay at a specific wavelength at 294 K:

$$\Omega_{294}(\lambda) \equiv \frac{I_{fast}(\lambda)}{I_{slow}(\lambda)} \qquad \text{(A-15)}$$

If, as assumed above, only the relaxed state line shape extends to 700 nm, $\Omega_{294}(\lambda)$ should approach a constant value as λ approaches 700 nm (see Figure 4). According to the kinetic model, this constant value is determined solely by the dynamics of the relaxed excited state and may be expressed as,

$$\mathcal{T} \equiv \Omega_{294}(700) = \frac{I_{fast}(700)}{I_{slow}(700)} = \frac{I_{Rel,fast}(700)}{I_{Rel,slow}(700)} \qquad \text{(A-16)}$$

where

$$I_{Rel,fast}(700) = g_{R*}(700)k_{f,R}\int_0^\infty \{\alpha\exp(-Xt) + \beta\exp(-\beta_1 t)\}\,dt$$

$$I_{Rel,slow}(700) = g_{R*}(700)k_{f,R}\int_0^\infty \gamma\exp(-\beta_2 t)\,dt$$

Thus, from the experimental quantities $\Omega_{294}(\lambda)$, $\Omega_{294}(700)$, and $I_{SS}(\lambda)$, the delayed relaxed, prompt relaxed, and vertical wavelength dependent emission probability functions are given by

$$I_{Rel,slow}(\lambda) = \frac{I_{SS}(\lambda)}{1 + \Omega_{294}(\lambda)} \qquad \text{(A-17)}$$

$$I_{Rel,fast}(\lambda) = \frac{I_{SS}(\lambda)\mathcal{T}}{1 + \Omega_{294}(\lambda)} \qquad \text{(A-18)}$$

$$I_{Vert}(\lambda) = \frac{I_{SS}(\lambda)[\Omega_{294}(\lambda) - \mathcal{T}]}{1 + \Omega_{294}(\lambda)} \qquad \text{(A-19)}$$

Division of $I_{Rel,slow}(\lambda)$ and $I_{Vert}(\lambda)$ by their respective integrals over all wavelengths generates the pure relaxed and vertical line shape functions g_{R*} and g_{V*}, respectively. These line shapes may be used to decompose the observed spectra into the vertical and relaxed emission components.